Systematic Development of Transmission-Line Models for Interconnects With Frequency-Dependent Losses

Karen M. Coperich, *Student Member, IEEE*, Jason Morsey, *Student Member, IEEE*, Vladimir I. Okhmatovski, *Member, IEEE*, Andreas C. Cangellaris, *Fellow, IEEE*, and Albert E. Ruehli, *Fellow, IEEE*

***Abstract*—This paper presents a new method for the extraction of the frequency-dependent, per-unit-length (p.u.l.) resistance, and inductance parameters of multiconductor interconnects. The proposed extraction methodology is based on a new formulation of the magneto-quasi-static problem that allows lossy ground planes of finite thickness to be modeled rigorously. The formulation is such that the p.u.l. impedance matrix for the multiconductor interconnect is extracted directly at a prescribed frequency. Once the matrix has been calculated over the bandwidth of interest, rational function representations of its elements are generated through a robust matrix curve-fitting process. Such a formulation enables subsequent transient analysis of interconnects through a variety of approaches. Direct incorporation of the rational function model into a general- purpose circuit simulator and a standalone multiconductor-transmission-line simulator is demonstrated.**

***Index Terms*—Broad-band transmission-line model, closed-form electromagnetic Green's functions, dispersion, dispersive multiconductor interconnect model, equivalent circuit, finite-difference time-domain simulation, frequency-dependent losses, frequency-dependent per-unit-length impedance matrix, frequency-dependent per-unit-length inductance parameters, frequency-dependent per-unit-length resistance parameters, high-speed electrical interconnections, lossy ground planes, magneto-quasi-static problem, method of moments, multiconductor transmission lines, ohmic losses, parameter-extraction methodology, planar inhomogeneous media, proximity effect, rational function representations, skin effect, SPICE-compatible models, telegrapher's equations, time-domain simulation, transmission line, vector curve fitting.**

I. Introduction

ACCURATE prediction of crosstalk levels and pulse distortion in high-speed interconnects is strongly dependent on the accuracy with which the ohmic loss-induced frequency dependence of the interconnect per-unit-length (p.u.l.) resistance and inductance parameters is modeled. Most of the existing interconnect transient simulators rely on basic skin-effect models for the conductors. Such models do not correctly capture the contribution of the proximity effect present in the current distribution in the interconnects. Thus, the frequency-dependent p.u.l. resistance results are only approximate. Furthermore, none of the existing models in commercially available transient simulators take into account the contribution of the ohmic loss in the reference ground path in the p.u.l. resistance of the conductors. It is well known that, at high frequencies, there is crowding of the current in the region of the return path immediately adjacent to the conductors. The extent of this crowding is frequency dependent. Consequently, not only does the return path contribute to the p.u.l. resistance, its contribution is also dependent on frequency.

In this paper, a new approach is proposed for the extraction of the frequency-dependent p.u.l. resistance and inductance parameters of multiconductor interconnects. The proposed approach combines a new formulation of the magneto-quasi-static electromagnetic model that describes frequency-dependent field penetration in the lossy conductors with a robust vector-fitting algorithm to generate rational function approximations to the elements of the p.u.l. impedance matrix of a multiconductor interconnect.

The mathematical formulation is presented first, with the emphasis placed on the attributes of the new frequency-dependent resistance and inductance extraction process. This is followed by the generation of the rational function approximations to the elements of the p.u.l. resistance and inductance matrices. Use of these rational function approximations for the development of SPICE-compatible models for transient interconnect simulation purposes is also discussed. The paper concludes with the presentation of numerical results from the application of the proposed extraction methodology and the dispersive interconnect simulation approach to the modeling of signal dispersion and crosstalk in multiconductor interconnects.

II. Magneto-Quasi-Static Green's Function

Fig. 1 below depicts the cross section of a uniform transmission line with N active conductors. Even though the specific cross section is of the microstrip type, where a single ground plane is used as the reference conductor, the proposed methodology is applicable to any one of the interconnect structures commonly encountered in practice. All conductors are assumed to be lossy, including the ground plane. According to standard generalized transmission-line theory, the objective is to extract

Manuscript received January 15, 2001. This work was supported in part by the Semiconductor Research Corporation under Contract 98-DJ-611 and by an IBM Faculty Partnership Award. The work of K. M. Coperich was supported under a Scientific Research Council Graduate Fellowship.

K. M. Coperich was with the Electrical and Computer Engineering Department, University of Illinois at Urbana-Champaign, Urbana, IL 61801 USA. She is now with Sandia National Laboratories, Albuquerque, NM 87123 USA.

J. Morsey, V. I. Okhmatovski and A. C. Cangellaris are with the Electrical and Computer Engineering Department, University of Illinois at Urbana-Champaign, Urbana, IL 61801 USA.

A. E. Ruehli is with the IBM T. J. Watson Research Center, Yorktown Heights, NY 10598 USA.

Publisher Item Identifier S 0018-9480(01)08680-X.

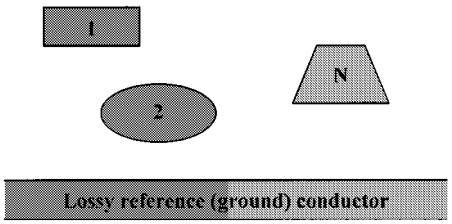

Fig. 1. Cross section of a uniform interconnect.

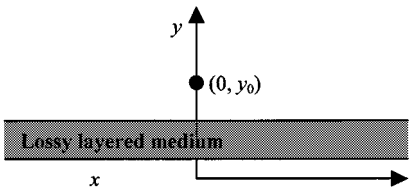

Fig. 2. Layered medium for the two-dimensional Green's function problem. The conductivity of the layered medium is, in general, y-dependent.

the p.u.l. frequency-dependent inductance and resistance matrices for the interconnect system.

Under the assumption of the quasi-TEM approximation [1], the extraction of the p.u.l. inductance and resistance matrices is based on the solution of a two-dimensional magneto-quasi-static boundary-value problem for the magnetic vector potential $\vec{A}(x, y) = \hat{z}A(x, y)$. Since the current flows only in the z-direction, the magnetic vector potential has only the z component. An expression for the electric current density inside one of the lossy conductors is obtained from Ohm's law and the equation that relates the electric field to the field potentials

$$J(x, y) = \sigma E(x, y) \Rightarrow$$
$$J(x, y) = \sigma \left[-j\omega A(x, y) - \frac{d\Phi}{dz} \right] \quad (1)$$

where σ is the electric conductivity, ω is the angular frequency, and Φ is the electric potential. Clearly, the time–harmonic variation $\exp(j\omega t)$ is assumed in this paper, and is suppressed for simplicity. The derivative of the electric potential is constant for each conductor for a given frequency of operation and system excitation. Using in (1) the integral form of $A(x, y)$ in terms of the current densities in the conductors, the following expression is obtained:

$$\frac{1}{\sigma} J(x, y) + j\omega \sum_{n=1}^{N} \iint_{S_n} G(x, y; x', y') J(x', y')\, ds' = -\frac{d\Phi}{dz} \quad (2)$$

where S_n denotes the cross section of the nth conductor. It is noted here that, in order to account for losses in the reference ground conductor, the current density throughout its cross section must also be calculated. However, for the case where such a reference conductor can be approximated by one of infinite planar extent, the calculation of the current distribution over its cross section can be avoided through a proper choice of the Green's function G in (2). This is explained below.

The Green's function G in (2) is the solution to the partial differential equation for the magnetic vector potential for the case where the source is a line current parallel to the z-axis. Without loss of generality, the line current is placed at a point $(0, y_0)$ on the y-axis. Thus, the governing equation assumes the form

$$\frac{\partial^2 G}{\partial x^2} + \frac{\partial^2 G}{\partial y^2} - j\omega \mu \sigma G = -\mu \delta(x)\delta(y - y_0). \quad (3)$$

With the lossy ground plane taken to be of infinite extent in the direction transversal to the y-axis, it is desirable to construct G in such a way that the presence of the lossy ground is accounted for. This way, there will be no need to solve for the current distribution within the lossy ground plane; yet its impact on the interconnect inductance and resistance will be taken into account. This is achieved by constructing G for the background geometry depicted in Fig. 2. The Green's function problem of interest is well known in applied electromagnetics as the layered medium problem. As shown in [2], analytic expressions for the Green's functions in such media are possible. However, they are in terms of slowly converging integrals.

Recently, a methodology has been proposed for the development of closed-form Green's functions for layered media [3]–[5]. Even though approximate, it has been shown in the aforementioned papers that the derived closed-form expressions provide excellent accuracy. It is this methodology that is used for the solution of (3). As depicted in Fig. 2, layered lossy substrates with position-dependent conductivity can be handled by the proposed method. Thus, in addition to its suitability for the effective modeling of lossy ground planes, the proposed methodology is an excellent candidate for the extraction of on-chip frequency-dependent interconnect parameters in the presence of lossy semiconductor substrates with variable doping.

The development begins with the derivation of the spectral-domain form of (3). More specifically, the Fourier-transform pair

$$G(x, y; y_0) = \frac{1}{2\pi} \int_{-\infty}^{\infty} g(\lambda, y; y_0) \exp(j\lambda x)\, d\lambda$$
$$g(\lambda, y; y_0) = \int_{-\infty}^{\infty} G(x, y; y_0) \exp(-j\lambda x)\, dx \quad (4)$$

is utilized to obtain, through the Fourier transform of (3), the differential equation for the spectral form $g(\lambda, y; y_0)$ of the Green's function

$$\frac{d^2 g}{dy^2} - j\omega\mu\sigma g - \lambda^2 g = -\mu\delta(y - y_0). \quad (5)$$

Even though analytic solutions for (5) are possible, they are in terms of exponential functions of the spectral variable λ. The inverse Fourier transforms of these functions cannot be done in closed form, and the numerical evaluation of the relevant integrals is expensive.

To circumvent this difficulty, a discrete solution of (5) is sought. For this purpose, the finite-difference (FD) method is employed. The discretization process is well known and will not be repeated here. The only issue that requires some discussion is the handling of the semiinfinite homogeneous media that extend to infinity in the positive and negative directions along

the y-axis. In the discrete model, these semiinfinite domains are mapped to finite ones, using the coordinate transformation of [6]. The specific details can be found in [3] and will not be repeated here. The FD approximation of (5) may be cast in the following matrix form:

$$(\mathbf{A} - \lambda^2 \mathbf{U})\mathbf{g} = -\mathbf{f} \tag{6}$$

where the matrix $\mathbf{A}$ is a tridiagonal matrix of dimension M equal to the number of interior nodes of the FD grid, $\mathbf{U}$ is the unity matrix of dimension M, and $\mathbf{g}$ is the vector of the unknown values of the spectral-domain Green's function at all of the FD nodes. The forcing vector $\mathbf{f}$ has all its elements equal to zero, except for the one at the row corresponding to the FD node where the source is located. Using the eigendecomposition $\mathbf{A} = \mathbf{TST}^{-1}$, the solution to (6) may be cast in the form

$$\mathbf{g} = \mathbf{T}(\mathbf{S} - \lambda^2 \mathbf{U})^{-1}\mathbf{r} \tag{7}$$

where $\mathbf{r} = -\mathbf{T}^{-1}\mathbf{f}$. Since $\mathbf{S}$ is diagonal, it follows immediately from the last equation that each element of the vector $\mathbf{g}$ is of the form

$$g_m = -\sum_{q=1}^{M} \frac{T_{mq} r_q}{\lambda^2 - s_q}. \tag{8}$$

In the last equation, the constants s_q, $q = 1, 2, \ldots, M$, depend only on the properties of the layered medium and the grid size. This is also true for the elements of the matrix $\mathbf{T}$. Finally, the elements of the vector $\mathbf{r}$ depend on the position of the source. This is the only vector that needs to be recalculated for different source locations.

The advantage of the result in (8) is that it allows for the inverse Fourier-transform integral to be calculated analytically. More specifically, the spatial-domain Green's function at node m is obtained from (8) through the following integration:

$$G(x, y_m; y_0) = -\frac{1}{2\pi} \int_{-\infty}^{\infty} \left(\sum_{q=1}^{M} \frac{T_{mq} r_q}{\lambda^2 - s_q} \right) \exp(j\lambda x)\, d\lambda. \tag{9}$$

Using contour integration techniques, it can be shown that

$$\int_{-\infty}^{\infty} \frac{\exp(j\lambda x)}{\lambda^2 - s_q}\, d\lambda = \frac{\pi}{j\sqrt{s_q}} \exp\left(-j\sqrt{s_q}|x|\right), \quad \mathrm{Im}\left(\sqrt{s_q}\right) < 0.$$

In view of this relationship (9) assumes the simple form

$$G(x, y_m; y_0) = \frac{j}{2} \sum_{q=1}^{M} (T_{mq} r_q) \frac{\exp\left(-j\sqrt{s_q}|x|\right)}{\sqrt{s_q}}. \tag{10}$$

Thus, the Green's function for the magneto-quasi-static problem in a layered medium is expressed in closed form, in terms of a finite sum of complex exponentials. The dependence on the y coordinates is built in the constant coefficients of the terms in the finite sum. The dependence on x appears explicitly in the argument of the exponentials.

From (10), it is seen that the number of summation terms is equal to the number of grid points in the FD grid. However, only a subset of these terms contributes significantly to the value of the Green's function. Adopting the approach in [5], the eigenvalues s_q are sorted so that $\sqrt{s_q}$ will have an increasingly negative imaginary part as q increases. As the summation in (10) is summed over q, the contribution from each $\exp(-j\sqrt{s_q}|x|)$ term becomes increasingly smaller. The series can then be truncated at $q < M$ when the additional terms reach some predetermined tolerance value. Since the exponential terms decay more rapidly with larger x, fewer terms are needed as the point of observation is further displaced from the source.

III. Extraction of Frequency-Dependent $\mathbf{R}$ and $\mathbf{L}$

The process for the extraction of the p.u.l. frequency-dependent resistance and inductance matrices for the multiconductor line begins with the discretization of its cross-sectional geometry and the numerical solution of the integral equation (2). Several approaches have been presented over the years in the literature for the numerical solution of this equation [7]–[10]. The approach presented here is a "volumetric" approach, where the conductor cross section is discretized into patches over which the current density is assumed to be constant. To be more concrete, let N_n be the number of patches in the cross section of conductor n, $n = 1, 2, \ldots, K$. Let $I_k^{(n)}$ be the total current flowing through patch k, $k = 1, 2, \ldots, N_n$, and let $a_k^{(n)}$ be the area of the kth patch. The current density over the kth patch is then given by $J_k^{(n)} = I_k^{(n)}/a_k^{(n)}$. The discretization of the cross sections is done in such a manner that the skin-effect behavior is resolved accurately at each frequency of interest. Thus, a finer grid is used along the perimeter of the conductor, with the grid size selected such that at the length of one skin depth is span by at least two elements. The grid size increases gradually toward the center of the conductor cross section.

With this notation, the method-of-moments approximation of (2) results in the following matrix representation for the discrete form of the integral equation:

$$(\mathbf{R}_p + j\omega \mathbf{L}_p)\, \mathbf{I}_p = -\mathbf{V}_p. \tag{11}$$

Each element R_{ij} of the full matrix $\mathbf{R}_p$ represents the p.u.l. resistance of filament i with respect to the current in filament j, where i and j may index filaments on separate conductors. The value of R_{ij} is computed by the expression in (12), where δ_{ij} is one if i equals j and zero, otherwise

$$R_{ij} = \frac{\delta_{ij}}{\sigma_i a_i} - \omega\, \mathrm{Im}\left[\frac{1}{a_i a_j} \iint_{S_i} \iint_{S_j} G(x_i, y_i; x_j, y_j)\, ds_i\, ds_j \right]. \tag{12}$$

Similarly, each element L_{ij} of the full matrix $\mathbf{L}_p$ represents the p.u.l. inductance of filament i with respect to the current in filament j, as shown in the following:

$$L_{ij} = \mathrm{Re}\left[\frac{1}{a_i a_j} \iint_{S_i} \iint_{S_j} G(x_i, y_i; x_j, y_j)\, ds_i\, ds_j \right]. \tag{13}$$

The Green's function $G(x_i, y_i; x_j, y_j)$ used in (12) and (13) accounts for the presence of any layered lossy media, in addition to any ground or reference plane losses, through the expression

in (10). The vector of unknowns $\mathbf{I}_p$ contains the filament currents

$$\mathbf{I}_p = \left\{ \mathbf{I}_{C1}^T, \mathbf{I}_{C2}^T, \ldots, \mathbf{I}_{CN}^T \right\}^T. \tag{14}$$

Each of the vectors $\mathbf{I}_{Cn}, n = 1, 2, \ldots, K$ contains the filament currents of the nth conductor. Finally, recognizing that the p.u.l. voltage drop is the same for all filaments in the same conductor, the vector $\mathbf{V}_p$ in (11) may be written in terms of the K voltage drops $V_n, n = 1, 2, \ldots, K$ as follows:

$$\mathbf{V}_p = \begin{bmatrix} \mathbf{1}_{N_1} & \mathbf{0}_{N_1} & \cdots & \mathbf{0}_{N_1} \\ \mathbf{0}_{N_2} & \mathbf{1}_{N_2} & \cdots & \mathbf{0}_{N_2} \\ \vdots & \vdots & \ddots & \vdots \\ \mathbf{0}_{N_N} & \mathbf{0}_{N_N} & \cdots & \mathbf{1}_{N_N} \end{bmatrix} \begin{bmatrix} V_1 \\ V_2 \\ \vdots \\ V_N \end{bmatrix} = \mathbf{P}\mathbf{V} \tag{15}$$

where $\mathbf{1}_{N_n}, n = 1, 2, \ldots, K$ is a column vector of ones of length N_n (equal to the number of filaments in conductor n), $\mathbf{0}_{N_n}, n = 1, 2, \ldots, K$ is a vector of zeros of length N_n, and the vector $\mathbf{V}$ contains the K p.u.l. voltage drops in the K conductors. From the above equations, the vector of filament currents can be written in terms of the p.u.l. voltage drops as follows:

$$\mathbf{I}_p = -\left(\mathbf{R}_p + j\omega\mathbf{L}_p\right)^{-1} \mathbf{P}\mathbf{V}. \tag{16}$$

Recognizing that the total current I_n in conductor n is given by $I_n = \mathbf{1}_{N_n}^T \cdot \mathbf{I}_{Cn}$, the vector $\mathbf{I}$ of the K net currents in the K conductors is obtained from (14) as follows:

$$\mathbf{I} = -\mathbf{P}^T \left(\mathbf{R}_p + j\omega\mathbf{L}_p\right)^{-1} \mathbf{P}\mathbf{V}. \tag{17}$$

From (17), it is immediately obvious that the p.u.l. impedance matrix of the K-conductor transmission line is given by

$$\mathbf{Z}_{\text{pul}} = \left[\mathbf{P}^T \left(\mathbf{R}_p + j\omega\mathbf{L}_p\right)^{-1} \mathbf{P}\right]^{-1}. \tag{18}$$

Finally, the frequency dependent p.u.l. resistance and inductance matrices for the K-conductor line are

$$\mathbf{R}_{\text{pul}}(\omega) = \text{Re}\left\{\mathbf{Z}_{\text{pul}}\right\} \quad \mathbf{L}_{\text{pul}}(\omega) = \frac{1}{\omega}\,\text{Im}\left\{\mathbf{Z}_{\text{pul}}\right\}. \tag{19}$$

IV. SPICE-Compatible Form of the p.u.l. MTL Impedance Matrix

According to [11], the SPICE-compatible model for a multiconductor transmission line (MTL) with frequency-dependent losses is developed from the semidiscrete approximation of the generalized telegrapher's equations, where the spatial derivatives for the transmission-line voltages and currents are approximated using a FD scheme. While in [11], compact differences were used to achieve a discrete approximation of high order, standard second-order accurate finite differences may also be used. To achieve a form compatible with the modified nodal analysis (MNA) formulation [12], the frequency-dependent elements of the p.u.l. impedance matrix of the MTL need to be cast in a closed form that corresponds to the response of a realizable passive circuit.

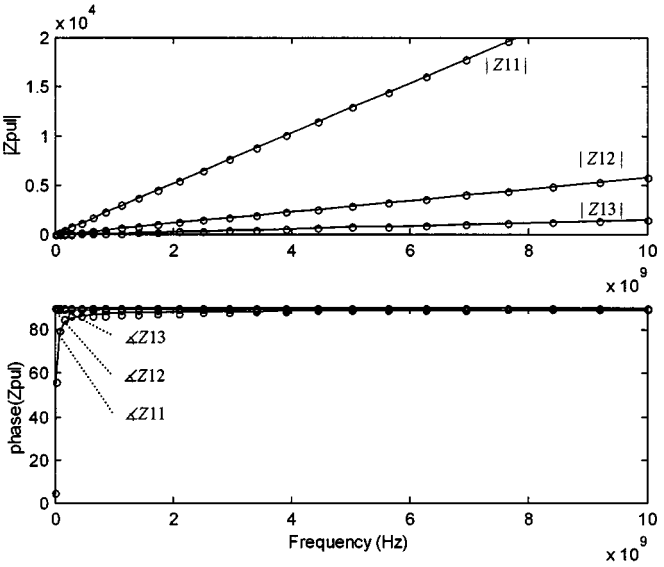

Fig. 3. Comparison between (18) and (20). The solid line represents the extracted p.u.l. impedance from (18), while the rational function approximation of (20) is indicated by the circle markers.

For the case of the frequency-dependent p.u.l. impedance matrix, the development of such a form is based on the modal network theory of the skin effect in lossy conductors [13]. According to this theory, the frequency dependence of the current distribution inside a lossy conductor can be described in terms of an equivalent network of resistors and inductors whose impedance is consistent with the form

$$\mathbf{Z}_{\text{pul}}(s) \cong \mathbf{R}_0 + s\mathbf{L}_0 + \sum_{q=1}^{Q_1} \frac{1}{s - P_q}\,\mathbf{R}_q \tag{20}$$

where $s = j\omega$. It is noted that the network is realizable if all P_q are negative, $\mathbf{R}_0$ is positive definite, and all of the elements of $\mathbf{L}_0$ are positive. For the sake of completeness, the dual closed form for the frequency-dependent admittance matrix $\mathbf{Y}_{\text{pul}} = \mathbf{G}_{\text{pul}} + s\mathbf{C}_{\text{pul}}$ is given by

$$\mathbf{Y}_{\text{pul}}(s) \cong \mathbf{G}_0 + s\mathbf{C}_0 + \sum_{q=1}^{Q_2} \frac{1}{s - B_q}\,\mathbf{G}_q. \tag{21}$$

However, for the examples in this paper, $\mathbf{G}_{\text{pul}}$ and $\mathbf{C}_{\text{pul}}$ are assumed to be independent of frequency. The representation of the p.u.l. impedance matrix in the form of (20) is achieved through the vector-fitting algorithm VECTFIT [14]. Using the frequency-dependent values of $\mathbf{Z}_{\text{pul}}$ calculated at several frequencies over the bandwidth of interest, VECTFIT fits simultaneously all elements in $\mathbf{Z}_{\text{pul}}$. VECTFIT makes no assumptions about the frequency dependence of the elements due to the generality of the form of (20). It was found that one pole was sufficient to capture the rather smooth frequency variation of the elements in the p.u.l. impedance matrix.

Fig. 3 depicts the elements of the first row of $\mathbf{Z}_{\text{pul}}$ for the coupled stripline geometry of Fig. 4. The stripline structure is vertically inhomogeneous due to the finite thickness and finite conductivity of the reference planes. The FD approximation of (5) discretizes the planar layered regions (bottom copper plane:

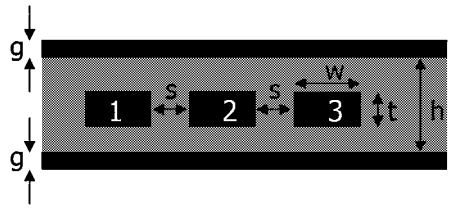

Fig. 4. Cross section of a stripline geometry where $s = 50\ \mu$m, $w = 50\ \mu$m, $t = 10\ \mu$m, $g = 10\ \mu$m, and $h = 200\ \mu$m. The relative dielectric constant $\varepsilon_r = 4$. All of the signal lines and reference conductors are copper metal.

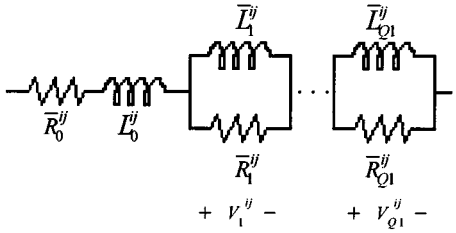

Fig. 5. Circuit representation of $Z_{\rm pul}^{ij}$.

$\sigma \neq 0$, inner dielectric: $\sigma = 0$, and top copper plane: $\sigma \neq 0$) so that the losses within the lossy reference planes are incorporated into the background media.

Once the p.u.l. impedance is cast into the SPICE-compatible and realizable form of (20), it can be rewritten as follows:

$$\mathbf{Z}_{\rm pul}(s) = \overline{\mathbf{R}}_0 + s\mathbf{L}_0 + \sum_{q=1}^{Q_1} \frac{s}{s - P_q}\,\overline{\mathbf{R}}_q$$

$$\overline{\mathbf{R}}_0 = \mathbf{R}_0 - \sum_{q=1}^{Q_1} \frac{1}{P_q}\mathbf{R}_q$$

$$\overline{\mathbf{R}}_q = \frac{1}{P_q}\,\mathbf{R}_q$$

$$\overline{\mathbf{L}}_q = -\frac{1}{P_q}\,\overline{\mathbf{R}}_q. \tag{22}$$

As s tends to zero in (22), all terms of $\overline{\mathbf{Z}}_{\rm pul}(s = 0)$ tend to zero, except $\overline{\mathbf{R}}_0$. Therefore, $\mathbf{Z}_{\rm pul}(s = 0) = \overline{\mathbf{R}}_0$ is the p.u.l. dc resistance, which means that it is a diagonal matrix. As s tends to infinity, the terms in the summation over q approach $\overline{\mathbf{R}}_q$. As a result, $\mathbf{L}_0$ is then the p.u.l. external inductance since the summation over q is purely resistive at high frequencies. Each element of $\mathbf{Z}_{\rm pul}$ can then be realized by the circuit shown in Fig. 5.

The p.u.l. equivalent circuit for each of the K conductors is shown in Fig. 6. The circuit is constructed by building upon the circuit in Fig. 5 for the self-impedance case ($i = j$). The addition of the off-diagonal elements of $\mathbf{L}_0$ is represented as mutual inductance coefficients

$$k^{ij} = \frac{L_0^{ij}}{\sqrt{L_0^{ii} L_0^{jj}}}, \qquad i \neq j. \tag{23}$$

The addition of the off-diagonal elements of $\overline{\mathbf{R}}_q$ is represented as a voltage-dependent voltage source E_i. Since the same set of poles are used in the characterization of every Z^{ij}, the off-diagonal elements of $\overline{\mathbf{R}}_q$ are proportional to each of the $(\overline{R}_q^{ii}, \overline{L}_q^{ii})$

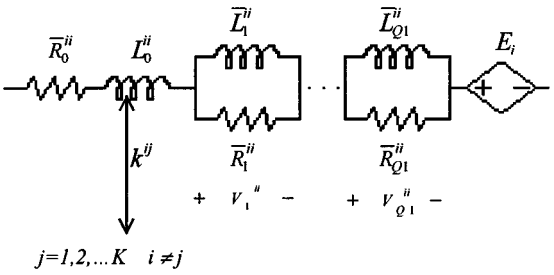

Fig. 6. Equivalent circuit for conductor i, accounting for resistive and inductive coupling.

pairs. As a result, the voltage drop V_q^{ij} is simply a scaling in magnitude of the voltage drop V_q^{jj}. Therefore, the voltage drop due to $\overline{R}_q^{ij}$ can be realized by

$$V_q^{ij} = \frac{\bar{R}_q^{ij}}{\bar{R}_q^{jj}}\,V_q^{jj}. \tag{24}$$

This now defines the coupling between off-diagonal residues by reusing the self-term circuit elements quantities from Fig. 5. The voltage source E_i is then the sum of voltage drops due to all coupled line residues or

$$E_i = \sum_{j=1}^{K} \sum_{q=1}^{Q1} V_q^{ij}, \qquad i \neq j. \tag{25}$$

The complex impedance of each conductor in a p.u.l. section of the MTL system is generically modeled by the circuit shown in Fig. 6. The model uses standard resistance, inductance, mutual inductance, and voltage-controlled voltage-source SPICE elements. It is important to emphasize that this SPICE-compatible p.u.l. equivalent circuit captures the frequency-dependent behaviors of $\mathbf{R}_{\rm pul}(\omega)$ and $\mathbf{L}_{\rm pul}(\omega)$ terms, including all off-diagonal coupling terms, for an MTL system.

V. Transient Simulation of the Dispersive MTL

The advantage of the pole/residue representations of (20) and (21) is that they facilitate the implementation of a variety of numerical schemes for transmission-line analysis both in the frequency and time domains. As already mentioned in the previous section, a SPICE-compatible subcircuit model, as shown in Fig. 6, can be synthesized from (20) and (21) in terms of lumped R, L, C, and G elements. Alternatively, standalone dispersive MTL simulators may also be devised. The development of such a simulator is described below.

The development begins with the discretization of the voltages and currents along the MTL in order to effect second-order accurate FD approximations of the spatial derivatives in the generalized telegrapher's equations

$$-\frac{\partial}{\partial z}\,\mathbf{V}(z, s) = \mathbf{Z}_{\rm pul}(s)\mathbf{I}(z, s)$$

$$-\frac{\partial}{\partial z}\,\mathbf{I}(z, s) = \mathbf{Y}_{\rm pul}(s)\mathbf{V}(z, s). \tag{26}$$

For this purpose, the unknown voltages and currents along the MTL are staggered in space, as shown in Fig. 7. Since each current node is placed at the center of two adjacent voltage

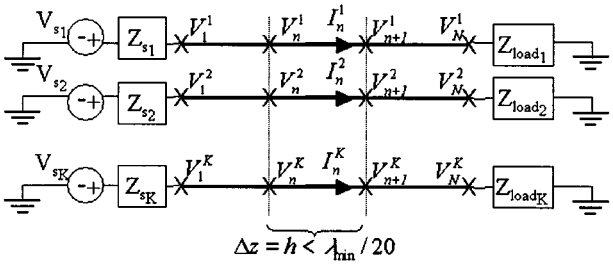

Fig. 7. Spatial discretization of the MTL voltages and currents.

nodes, the resulting discrete model is also reminiscent of the partial element equivalent circuit (PEEC) discretization of conductors. When the p.u.l. impedance and admittance matrices on the right-hand side of (26) are replaced by their equivalent closed-form expressions in (20) and (21), the following terms result:

$$\sum_{j=1}^{K} Z_{ij}(s) I_j(s) = \left[\sum_{j=1}^{K} \left(R_0^{(ij)} + sL_0^{(ij)}\right) I_j(s)\right] + \sum_{j=1}^{K}\sum_{q=1}^{Q_1} R_q^{(ij)} \frac{1}{s - P_q} I_j(s)$$

$$\sum_{j=1}^{K} Y_{ij}(s) V_j(s) = \left[\sum_{j=1}^{K} \left(G_0^{(ij)} + sC_0^{(ij)}\right) V_j(s)\right] + \sum_{j=1}^{K}\sum_{q=1}^{Q_2} G_q^{(ij)} \frac{1}{s - B_q} V_j(s). \quad (27)$$

The terms in the brackets on the right-hand side of the equations are familiar and describe the resistive, inductive, conductive, and capacitive coupling between the conductors in the specific spatial segment. Lumped-element representations for them are straightforward. The remaining terms can be written in a much simpler form by introducing the following auxiliary vectors:

$$\mathbf{I}_j^{(q)}(s) = \frac{1}{s - P_q}\mathbf{I}_j(s), \qquad q = 1, 2, \ldots, Q_1$$

$$\mathbf{V}_j^{(q)}(s) = \frac{1}{s - B_q}\mathbf{V}_j(s), \qquad q = 1, 2, \ldots, Q_2. \quad (28)$$

It was shown in the previous section that the terms in (28) directly lead to a SPICE-compatible equivalent-circuit representation of dependent current and voltage sources. Alternatively, the inverse Laplace transforms of these expressions yield the following convolution relationships:

$$\mathbf{I}_j^{(q)}(t) = \exp(P_q t) * \mathbf{I}_j(t), \qquad q = 1, 2, \ldots, Q_1$$

$$\mathbf{V}_j^{(q)}(t) = \exp(B_q t) * \mathbf{V}_j(s), \qquad q = 1, 2, \ldots, Q_2. \quad (29)$$

Efficient recursive schemes are available for the implementation of these convolutions [15]. Utilizing (29) in the time-domain form of (28), a leapfrog time-integration scheme is used for the transient analysis of the MTL. The update equations are as follows:

$$\mathbf{V}_n^{(m+1)\Delta t} = \left[(h/\Delta t)\mathbf{C}_0 + (h/2)\mathbf{G}_0\right]^{-1} \cdot \left[\left((h/\Delta t)\mathbf{C}_0 - (h/2)\mathbf{G}_0\right)\mathbf{V}_n^{(m)\Delta t} + \left(\mathbf{I}_{n-1}^{(m+1/2)\Delta t} - \mathbf{I}_n^{(m+1/2)\Delta t}\right)\right]$$

$$\mathbf{I}_n^{(m+3/2)\Delta t} = \left[(h/\Delta t)\mathbf{L}_0 + (h/2)\mathbf{R}_0 + (h/2)\mathbf{S}\right]^{-1} \cdot \left[\begin{array}{l}\left((h/\Delta t)\mathbf{L}_0 - (h/2)\mathbf{R}_0 - (h/2)\mathbf{S}\right)\mathbf{I}_n^{(m+1/2)\Delta t} \\ + \left(\mathbf{V}_n^{(m+1)\Delta t} - \mathbf{V}_{n+1}^{(m+1)\Delta t}\right) + \sum_q \mathbf{R}_q e^{P_q \Delta t}\mathbf{C}_{n,q}^{m\Delta t}\end{array}\right]$$

$$\mathbf{S} = -\sum_q \frac{1}{P_q}\left(1 - e^{P_q \Delta t}\right)\mathbf{R}_q$$

$$\mathbf{C}_{n,q}^{m\Delta t} = e^{P_q \Delta t}\mathbf{C}_{n,q}^{(m-1)\Delta t} - \frac{1}{2P_q}\left(1 - e^{P_q \Delta t}\right)\left(\mathbf{I}_n^{(m+1/2)\Delta t} + \mathbf{I}_n^{(m-1/2)\Delta t}\right). \quad (30)$$

In addition, the equations

$$\mathbf{I}_{R_s}^{(m+1/2)\Delta t} = \left[(1/2)\mathbf{R}_s\right]^{-1}\left[\begin{array}{l}\left(\mathbf{V}_s^{(m+1)\Delta t} + \mathbf{V}_s^{(m)\Delta t}\right) \\ - \left(\mathbf{V}_1^{(m+1)\Delta t} - \mathbf{V}_1^{(m)\Delta t}\right)\end{array}\right]$$

$$\mathbf{I}_{C_l}^{(m+1/2)\Delta t} = \left[(1/\Delta t)\mathbf{C}_l\right]\left[\left(\mathbf{V}_N^{(m+1)\Delta t} - \mathbf{V}_N^{(m)\Delta t}\right)\right] \quad (31)$$

are used to update the voltages $\mathbf{V}_{n=1}^{(m+1)\Delta t}$ and $\mathbf{V}_{n=N}^{(m+1)\Delta t}$ at the near and far ends of the MTL, respectively. Even though (31) is written for the specific cases where linear voltage sources are connected at the near end and capacitors are connected at the far end, discrete approximations for the time-dependent voltage–current relationship of any type of lumped elements could have been used.

The selection of the time and spatial discretizations Δt and h are designated by the user prior to performing the time-domain simulation. If the wave phenomena is sufficiently sampled (i.e., $h \leq \lambda_{\min}/10$) and the courant stability condition is met, no long-time instabilities were observed.

VI. Numerical Implementation

In order to demonstrate the numerical implementation of the proposed methodology, the interconnect stripline of Fig. 4 was analyzed using the driving and termination conditions indicated in Fig. 7. All conductors were assumed to be copper with conductivity 5.8×10^7 S/m. The elements of the p.u.l. capacitance matrix are $C11 = C33 = 1.1649$ pF/cm, $C22 = 1.2407$ pF/cm,

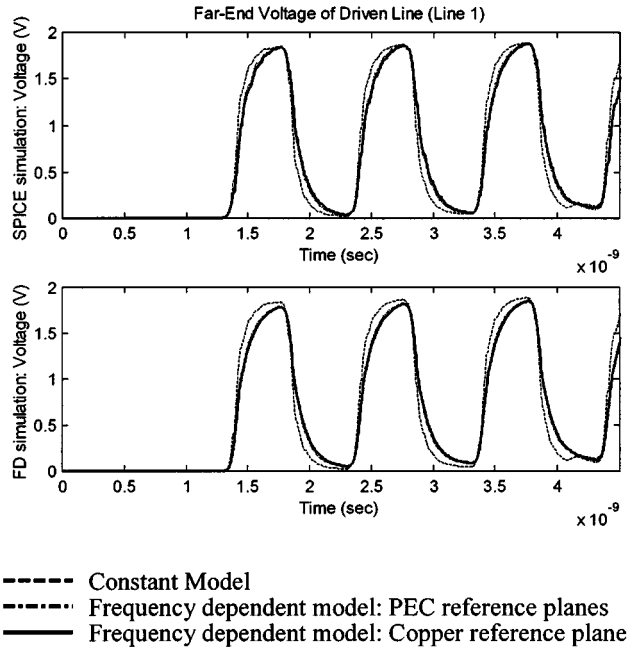

Fig. 8. Far-end voltage waveform on the driven line (line 1). The dashed line shows the results of the constant model where the p.u.l. inductance matrix and dc p.u.l. resistance were used. The solid and dashed–dotted lines show the responses of the frequency-dependent model of (18). Top: SPICE simulations using the technique of Section IV. Bottom: FD simulations using the technique of Section V.

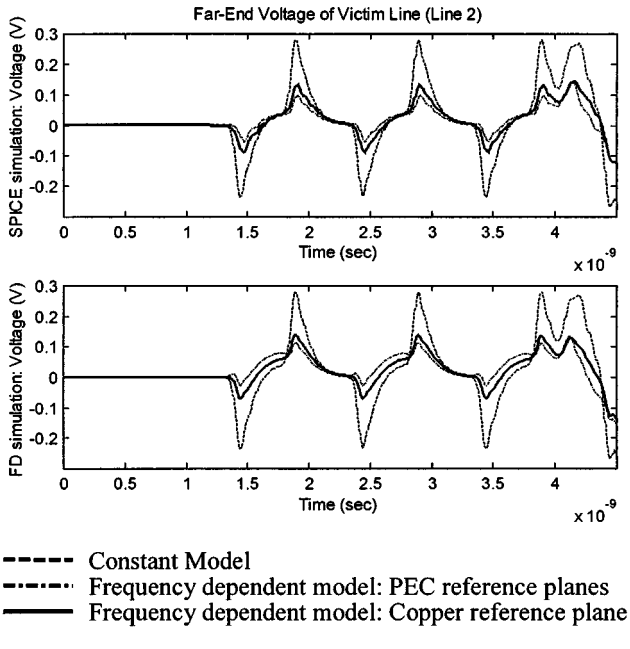

Fig. 9. Far-end voltage waveform on the victim line (line 2). The dashed line shows the results of the constant model where the p.u.l. inductance matrix and dc p.u.l. resistance were used. The solid and dashed–dotted lines show the responses of the frequency-dependent model of (18). Top: SPICE simulations using the technique of Section IV. Bottom: FD simulations using the technique of Section V.

$C12 = C21 = C23 = C32 = -0.2678$ pF/cm, and $C13 = C31 = -0.0083$ pF/cm. The source waveform is a trapezoidal pulse train of amplitude 2 V, a period of 1 ns, a 50% duty cycle, and rise and fall times of 50 ps. Lines 1 and 3 are driven by a voltage source with a matched input resistance. The input of the quiet line, i.e., line 2, is shorted to ground. All three lines are 20-cm long and terminated into 1-pF capacitors.

In order to evaluate the impact and necessity of taking into account the frequency-dependence of the p.u.l. resistance and inductance matrices, the time-domain responses of the system are compared with those obtained when the frequency dependence is not taken into account. For the frequency-independent simulation, the p.u.l. resistance is set equal to the dc resistance of each line while the p.u.l. inductance matrix is taken to be that obtained under the assumption of perfect conductors (i.e., neglecting the internal inductance of any conductor with finite conductivity). Figs. 8 and 9 compare the multiline far-end transient responses generated by the constant and frequency-dependent models.

The impact of the frequency dependence of the p.u.l. resistance and inductance both on the rise time (and, hence, delay) of the received signal and its amplitude is evident. Fig. 10 helps explain this significant discrepancy by providing a comparison of the frequency-dependent p.u.l. resistance and inductance of a single conductor between two closely spaced copper and perfect electric conductor (PEC) reference planes. At the upper end of the frequency bandwidth of interest, the frequency-dependent resistance is 3–7 times larger than its dc value and an additional 25%–35% larger for a copper reference plane. Consequently, the high-frequency portion of the pulse spectrum,

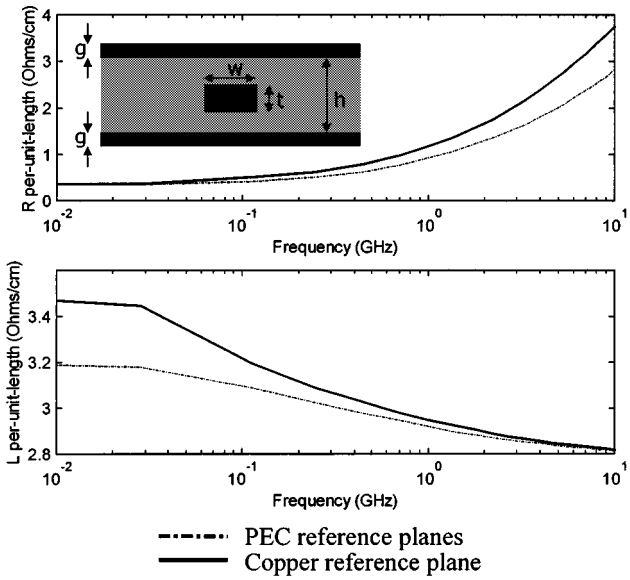

Fig. 10. Frequency dependence of the p.u.l. resistance (top) and inductance (bottom) of the single stripline configuration with $w = 50\ \mu$m, $t = 10\ \mu$m, $g = 10\ \mu$m, and $h = 100\,\mu$m.

which shapes the rising and falling sides of the pulse, is suffering higher attenuation that the low-frequency portion. Figs. 8 and 9 display the signal distortion that results from this type of high-frequency attenuation. As a result, there is a significant difference in the delays of the responses generated by the constant and frequency-dependent models. Fig. 10 also illustrates the additional inductance present in conductors when the frequency of operation is not high enough to constrict the current flow

solely near the conductor surface. The figure illustrates that the low-frequency inductance can be 20% larger then the high-frequency inductance. Also, the extracted inductance values incorporating a copper reference plane are 10% larger than the PEC reference plane case of Fig. 10. Since the inductance directly affects the velocity of propagation of a signal, its frequency dependency results in dispersion (or spreading) of time-domain responses. Evidence of this type of signal distortion can be seen in Figs. 8 and 9. Fig. 10 also shows the sizeable change in $\mathbf{R}_{\rm pul}(\omega)$ and $\mathbf{L}_{\rm pul}(\omega)$ values between PEC and copper reference planes. Some evidence of this is seen in Figs. 8 and 9; however, Fig. 10 highlights the discrepancy between reference plane models for a geometry with a much thinner dielectric substrate.

As the vertical separation between reference planes decreases, a system of conductors becomes more tightly coupled. The physical spacing between signal conductors relative to the distance between the reference planes determines the current return path. Since the coupling amongst a system of conductors will simultaneously depend on the layout (broadside versus edge side), width (w), thickness (t), height (h), and spacing (s) of the conductors, a complete phenomenological study is necessary and already underway.

Throughout the results shown in Figs. 8 and 9, the SPICE simulation results using the equivalent circuit of Section IV were presented along with results from the dispersive FD technique of Section V. The agreement between the waveforms computed from these two methods is very good. The flexibility of the $\mathbf{Z}_{\rm pul}$ representation of (20) to lend itself to multiple analysis techniques is a significant benefit to the extraction-fitting process described in this paper.

VII. Concluding Remarks

In summary, a new approach has been introduced for the development of SPICE-compatible models for high-speed interconnections exhibiting dispersion due to ohmic loss. The new approach combines a rigorous modeling of the frequency dependence of the field penetration inside the lossy conductors with a versatile curve-fitting scheme to develop equivalent *R–L* circuits that describe the frequency dependence of the p.u.l. impedance matrix for an MTL.

These models are subsequently combined with semidiscrete approximations of telegrapher's equation to generate SPICE-compatible models for the dispersive MTL. This equivalent-circuit model and its accompanying transient SPICE simulations build upon the results presented in [16] and [17].

The emphasis of the numerical application was on interconnects where the loss was solely due to the ohmic loss in the signal and reference conductors. Hence, only the p.u.l. inductance and resistance matrices were frequency dependent. However, the proposed model can also handle the general case where the p.u.l. conductance and capacitance matrices exhibit frequency dependence as well. Interconnects with such behavior will be examined in a future paper.

References

[1] R. E. Collin, *Field Theory of Guided Waves*. New York: IEEE Press, 1991.

[2] J. R. Wait, *Geo-Electromagnetics*. New York: Academic Press, 1982.

[3] A. C. Cangellaris, "A new methodology for the direct generation of closed-form electrostatic Green's functions in layered dielectrics," in *Proc. 16th Annu. Rev. Progress Appl. Comput. Electromag.*, Monterey, CA, May 2000, pp. 108–114.

[4] A. C. Cangellaris and V. I. Okhmatovski, "New closed-form Green's function in shielded planar dielectric media," *IEEE Trans. Microwave Theory Tech.*, to be published.

[5] V. I. Okhmatovski and A. C. Cangellaris, "A new technique for the derivation of closed-form electromagnetic Green's functions for unbounded planar layered media," Center Comput. Electromag., ECE Dept., Univ. Illinois at Urbana-Champaign, Res. Rep. CCEM-14-00, Sept. 2000.

[6] C. E. Grosch and S. A. Orszag, "Numerical solution of problems in unbounded regions: Coordinate transforms," *J. Comput. Phys.*, vol. 25, pp. 273–296, 1977.

[7] C. S. Yen, Z. Fazarinc, and R. L. Wheeler, "Time-domain skin-effect model for transient analysis of lossy transmission lines," *Proc. IEEE*, vol. 70, pp. 750–757, July 1982.

[8] M. J. Tsuk and A. J. Kong, "A hybrid method for the calculation of the resistance and inductance of transmission lines with arbitrary cross sections," *IEEE Trans. Microwave Theory Tech.*, vol. 39, pp. 1338–1347, Aug. 1991.

[9] S. Kim, B. T. Lee, E. Turner, and D. Neikirk, "Efficient internal impedance method for series impedance calculation of lossy transmission lines: Comparison to standard impedance boundary condition," *IEEE Trans. Microwave Theory Tech.*, to be published.

[10] K. M. Coperich, A. Ruehli, and A. C. Cangellaris, "Enhanced skin effect for partial-element equivalent-circuit (PEEC) models," *IEEE Trans. Microwave Theory Tech.*, vol. 48, pp. 1435–1442, Sept. 2000.

[11] S. Pasha, M. Celik, A. C. Cangellaris, and J. Prince, "Passive SPICE-compatible models of dispersive interconnects," in *Proc. 49th Electron. Comp. Technol. Conf.*, San Diego, CA, 1999, pp. 493–499.

[12] C. Ho, A. Ruehli, and P. Brennan, "The modified nodal approach to network analysis," *IEEE Trans. Circuits Syst.*, vol. CAS-22, pp. 504–509, June 1975.

[13] P. Silvester, "Model network theory of skin effect in flat conductors," *Proc. IEEE*, vol. 54, pp. 1147–1151, Sept. 1966.

[14] B. Gustavsen and A. Semlyen, "Rational approximation of frequency domain responses by vector fitting," *IEEE Trans. Power Delivery*, vol. 14, pp. 1052–1061, July 1999.

[15] S. Lin and E. S. Kuh, "Transient simulation of lossy interconnects based on recursive convolution formulation," *IEEE Trans. Circuits Syst. I*, vol. 39, pp. 879–892, Nov. 1992.

[16] K. M. Coperich, J. Morsey, V. Okhmatovski, A. C. Cangellaris, and A. E. Ruehli, "Systematic development of transmission line models for interconnects with frequency-dependent losses," in *Proc. 9th Elect. Performance Electron. Packag. Topical Meeting*, Phoenix, AZ, 2000, pp. 221–224.

[17] J. Morsey, K. M. Coperich, V. Okhmatovski, A. C. Cangellaris, and A. E. Ruehli, "A new broadband transmission line model for accurate simulation of dispersive interconnects," in *Proc. 3rd Electron. Packag. Technol. Conf.*, Singapore, 2000, pp. 345–351.

Karen M. Coperich (S'90) received the B.S. degree in electrical engineering (*magna cum laude*) from the University of Maryland at College Park, in 1994, the M.S. degree in electrical engineering from the University of Illinois at Urbana-Champaign, in 1996, and the Ph.D. degree in electrical engineering from the University of Illinois at Urbana-Champaign, in 2001.

She was with the National Aeronautics and Space Administration (NASA) Goddard Space Flight Center. She has held internships at Motorola and IBM. She is currently a Member of the Technical Staff at Sandia National Laboratories, Albuquerque, NM. Her research interests include electromagnetic modeling of high-speed on-chip interconnects, model order reduction techniques, signal integrity analysis, advanced microwave measurements, and interdisciplinary applications.

Dr. Coperich is a member of Eta Kappa Nu and Tau Beta Pi. She is a fellow of the National Science Foundation. Her doctoral research was supported under the Graduate Fellowship Program of the Semiconductor Research Corporation, courtesy of National Semiconductor Incorporated. She was the recipient of both campus and the Department of Electrical and Computer Engineering, University of Illinois at Urbana-Champaign awards for her accomplishments as an instructor.

Jason Morsey (S'01) received the B.S. degree in electrical engineering (*cum laude*) and the M.S. degree in electrical engineering from Clemson University, Clemson, SC, in 1998 and 2000, respectively, and is currently working toward the Ph.D. degree at the University of Illinois at Urbana-Champaign.

He was a co-op student with Reliance Electric and W. R. Grace. His research was focused on near-field antennas. His current research interests include electromagnetic modeling of high-speed on-chip interconnects and signal integrity analysis.

Vladimir I. Okhmatovski (M'99) was born in Moscow, Russia, in 1974. He received the M.S. (with distinction) and Candidate of Science (Ph.D.) degrees from the Moscow Power Engineering Institute, Moscow, Russia, in 1996 and 1997, respectively.

In 1997, he joined the Radio Engineering Department, Moscow Power Engineering Institute, as an Assistant Professor. From 1998 to 1999, he was a Post-Doctoral Fellow in the Microwave Laboratory, National Technical University of Athens, Athens, Greece. In 1999, he joined the Department of Electrical and Computer Engineering, University of Illinois at Urbana-Champaign, where he is currently a Post-Doctoral Research Associate. He has authored or co-authored over 20 papers in professional journals and conference proceedings. His research interest include geometrical and physical theories of diffraction, conformal antennas and arrays, fast algorithms in computational electromagnetics, and modeling of high-speed interconnects.

Dr. Okhmatovski was the recipient of a 1995 scholarship of the Government of the Russian Federation, a 1996 scholarship of the President of the Russian Federation, and a 1997–2000 scholarship of the Russian Academy of Science. In 1996, he received Second Prize for the Best Young Scientist Report presented at the VI International Conference on Mathematical Methods in Electromagnetic Theory (MMET'96).

Andreas C. Cangellaris (M'86–SM'97–F'00) received the Diploma degree in electrical engineering from the University of Thesalloniki, Thesalloniki, Greece, in 1981, and the M.S. and Ph.D. degrees in electrical engineering from the University of California at Berkeley, in 1983 and 1985, respectively.

He is currently a Professor of electrical and computer engineering at the University of Illinois at Urbana-Champaign. From 1987 to 1997, he was with the Department of Electrical and Computer Engineering, University of Arizona. From 1985 to 1987, he was a Senior Research Engineer in the Department of Electronics Engineering, General Motors Research Laboratories, Warren, MI. His research interests and contributions are in two major areas. The first is the area of applied computational electromagnetics. The second is the area of modeling and simulation for high-speed interconnection and package electrical analysis. He has authored or co-authored over 100 scientific journal and conference papers in these areas.

Prof. Cangellaris is co-founder of the IEEE Topical Meeting on Electrical Performance of Electronic Packaging, which is sponsored jointly by the IEEE Microwave Theory and Techniques Society (IEEE MTT-S) and the IEEE Components, Packaging and Manufacturing Technology Society. He served as the meeting co-chair for the first three years. Since then, he has served as a member of its Technical Program Committee. This meeting is considered the premier conference on package electrical analysis and design. He is also an active participant in the Electronic Components and Technology Conference (ECTC), as a member of the Technical Program Subcommittee on Modeling and Simulation. In addition, he serves as a member of the Technical Program Committee for the IEEE MTT-S International Microwave Symposium. In 1998, he was the general chairman for the 8th Biennial Conference on Electromagnetic Field Computation, Tucson, AZ, which is sponsored by the IEEE Magnetics Society.

Albert E. Ruehli (M'65–SM'74–F'84) received the Ph.D. degree in electrical engineering from the University of Vermont, Burlington, in 1972.

He has been a member of various projects with IBM, including mathematical analysis, semiconductor circuits and devices modeling, and as manager of a very large scale integration (VLSI) design and computer-aided design (CAD) group. Since 1972, he has been with the IBM T. J. Watson Research Center, Yorktown Heights, NY, where he currently a Research Staff Member in the Electromagnetic Analysis Group. He edited *Circuit Analysis, Simulation and Design* (New York, North Holland, 1986, 1987) and authored or co-authored of over 100 technical papers.

Dr. Ruehli is a member of the Society for Industrial and Applied Mathematics (SIAM). He has served in numerous capacities for the IEEE. He has also been a member of the IEEE Circuit and System Society AdCom. He is an associate editor for the IEEE TRANSACTIONS ON COMPUTER-AIDED DESIGN OF INTEGRATED CIRCUITS AND SYSTEMS. He has given numerous talks at universities including keynote addresses and tutorials at conferences, and has organized many sessions. He was the recipient of the IBM Outstanding Contribution Awards (1975, 1978, 1982, 1995), and the 1982 Guillemin-Cauer Prize Award for his work on waveform relaxation and 1999 Golden Jubilee Medal, both presented by the IEEE Circuits and Systems Society.